DATA REPOSITORY ITEM 2013321

For

Iron formation carbonates: Paleoceanographic proxy or recorder of microbial diagenesis?

Clark M. Johnson[1,2*], James M. Ludois[1,2], Brian L. Beard[1,2],
Nicolas J. Beukes[3], and Adriana Heimann[4]

EXPLANATORY DETAIL FOR FIGURE 1

Isotopic compositions for carbonates in equilibrium with seawater are calculated using the following sources and assumptions. $^{87}Sr/^{86}Sr$ uses the curves from Veizer (1989) and Shields and Veizer (2002). $\delta^{56}Fe$ assumes a seawater composition of zero and uses the siderite-$Fe(II)_{aq}$ fractionation factor of Wiesli et al. (2004). $\delta^{13}C$ assumes a seawater composition of zero and uses the carbonate-water fractionation factors of Jimenez-Lopez et al. (2001) and Jimenez-Lopez and Romanek (2004). $\delta^{18}O$ values for carbonates in equilibrium with seawater assumes the seawater $\delta^{18}O$ lay between −1 and −4 ‰ and a temperature of 50 °C; such a temperature lies between the extremes estimated for the early Precambrian oceans and accounts for the possibility for moderate early diagenesis (assuming isotopic equilibrium is maintained with ambient seawater). Lower temperatures will increase the $\delta^{18}O$ calculated for carbonates, and higher temperatures will decrease the $\delta^{18}O$ calculated for carbonates. Carbonate-water O isotope fractionation factors from Carothers et al. (1988) and Kim and O'Neil (1997).

EXPLANATORY DETAIL FOR FIGURE 2

Compilation of isotopic and chemical data for the Neoarchean to Paleoproterozoic Kuruman and Gamohaan formations. Increasing Fe contents upwards correlates with the transition from the Gamohaan to Kuruman formations, although one ferruginous shale that has anomalously high Fe contents is found in the upper Gamohaan Formation (Beukes et al., 1990). Iron contents and isotopic compositions, as well as C and O isotope compositions from previous studies. Rb-Sr data for the Kuruman and Gamohaan formations mostly from this study, with additional Rb-Sr data from the Gamohaan Formation from Kamber and Webb (2001). Stratigraphic section referenced to core AD-5; additional data from other drill core projected onto AD-5, referenced to the base of the Kuruman Iron Formation and thickness of the Tsineng member of the Gamohaan Formation. Data from Beukes et al. (1990; cores AD-5, WB-98, DI-1), Beukes and Klein (1990; core CN-109), Kaufman (1996; cores AD-5, WB-98, and DI-1), Kamber and Webb (2001; unnamed core S of Kuruman), Johnson et al. (2003; core AD-5), von Blanckenburg et al. (2008; unnamed core S of Kuruman), Fischer et al. (2009; core BH 1-SACHA), Heimann et al. (2010; cores AD-5, WB-98, DI-1), and this study (cores AD-5, WB-98, DI-1).

SAMPLES AND ANALYTICAL METHODS

Three stratigraphically equivalent drill cores that encompass the platform section of the Kuruman BIF were analyzed (AD-5, DI-1, WB-98). A detailed description of the geologic setting, stratigraphy, lithology, and geochemistry of the cores analyzed is given in Klein and Beukes (1989) and Beukes and Klein (1990). Both carbonates (Table DR-1) and interbedded shales (Table DR-2) were analyzed for ^{87}Rb-^{87}Sr isotopes in the cores, and shales were additionally analyzed for Nd isotopes and REE contents (Table DR-2).

Carbonate sampling

Sampling methods are outlined in Heimann et al. (2010), as are details on the petrography of the samples. The ^{87}Rb-^{87}Sr isotope analyses were done on the washes that contained Rb and Sr from the Fe ion-exchange chemistry done by Heimann et al. (2010). Milligram-size powders of sampled carbonates were obtained using a tungsten carbide scribe, and were split, one for C and O isotope analysis, and the other for Fe and ^{87}Rb-^{87}Sr isotope analysis. A detailed description of C, O, and Fe isotope analysis methods is given by Heimann et al. (2010). Detailed microsampling of individual laminae was critical for evaluating isotopic heterogeneity on a fine scale, which, for Rb-Sr, assess Sr residence time, an independent check on expected equilibrium with seawater. Therefore, typical microsampling produced only ~ 1 mg of carbonate powder for Fe and ^{87}Rb-^{87}Sr analysis, which is an exceptionally small quantity as compared to most ^{87}Rb-^{87}Sr isotope studies of carbonates. Such small quantities were not amenable to Nd isotope or REE analysis.

Carbonate powders were totally dissolved in high molarity distilled HCl, spiked with a mixed ^{84}Sr-^{87}Rb tracer for determination of Rb and Sr contents by isotope dilution, followed by Fe separation. It is important to note that partial digestion approaches, such as mild treatment with acetic acid, was not possible because: 1) such approaches may compromise Fe isotope analysis (Valaas-Hyslop et al., 2008), and 2) siderite is resistant to dissolution in acetic acid. Moreover, leaching procedures may potentially fractionate Rb/Sr ratios, and so were not employed. For 2.5 b.y.-old samples, even slight changes in Rb/Sr ratios may markedly affect the calculated initial $^{87}Sr/^{86}Sr$ ratios.

The remaining cations from the Fe ion-exchange columns underwent separation of Sr and Rb, where Sr was separated using Sr spec® resin and HNO_3 as the mobile phase. Rubidium was separated using cation exchange chromatography (BioRad AG-MP-50 100-200 mesh resin) and HCl as the mobile phase. To ensure low total procedural blanks, the Sr spec® resin was first cleaned using procedures from Charlier et al. (2006). Average procedural blanks were 137 pg of Sr and 50 pg of Rb. Because sample size was very small (~ 0.001 g) and Sr concentrations were low (down to ~1 ppm) in the iron-rich carbonate minerals, typical analyses involved only ~ 5 ng Sr. Nevertheless, Sr blank contributions were negligible (see below).

Strontium isotope analyses of carbonates were made using a VG Instruments *Sector 54* thermal ionization mass spectrometer (TIMS) in the Radiogenic Isotope Laboratory at the University of Wisconsin-Madison, using a 3-jump multi-dynamic analysis method. Strontium was loaded following the methods of Charlier et al. (2006) using single Re filaments, with

H_3PO_4 and TaF activator, and Sr isotope ratios were exponentially normalized to a $^{86}Sr/^{88}Sr = 0.1194$. A typical analysis consisted of 120 ratios and an ^{88}Sr ion intensity between 1-3 x 10^{-11} amps. Using the above method, 20 analyses of NIST SRM-987 Sr using 2-10 ng of Sr per analysis yielded an $^{87}Sr/^{86}Sr$ ratio of 0.71026±0.00003 (n=20; 2-SD). The measured $^{87}Sr/^{86}Sr$ ratios ($^{87}Sr/^{86}Sr_{m)}$ of the BIF carbonates were corrected to initial $^{87}Sr/^{86}Sr$ ratios, defined as $^{87}Sr/^{86}Sr_i$, using the depositional age of the Kuruman Iron Formation given by Beukes and Gutzmer (2008) of 2480±10 Ma.

Because each sample had very low quantities of Rb, typically 1 ng, Rb analyses were performed using a single Daly detector peak-hopping mode, and the average $^{87}Rb/^{85}Rb$ is based on 30 ratios. The measured $^{87}Rb/^{85}Rb$ of NIST SRM-984 was 0.3803±0.0042 (n=12; 2-SD) on 1 ng loads of Rb run under similar conditions as samples. Relative to the certified Rb isotope composition of NIST SRM-984 ($^{87}Rb/^{85}Rb$=0.386±0.002), this produces an exponential β correction factor (Wasserburg et al., 1981) of 0.5682, and this correction factor was applied to the measured $^{87}Rb/^{85}Rb$ ratios obtained on samples.

Because some of the samples that were analyzed had very low total Sr contents (~1 ng Sr), it is possible that some of our measured $^{87}Sr/^{86}Sr$ ratios could be affected by procedural blanks, which averaged 0.137 ng (9 total Sr procedural blanks were analyzed, and the values were 285, 60, 53, 70, 89, 55, 409, 161, and 58 pg). On average, these blank levels are less than 1.5% of the total sample Sr content of siderite/ankerite. Rubidium total procedural blanks were 51, 17, 29, 18, 4, 192, 100, 22, and 13 pg, which, on average, are less than 1% of the total Rb content of siderite/ankerite that was analyzed. Virtually all of the Sr procedural blank is from HCl, and we analyzed 200 ml of distilled HCl that had been evaporated under HEPA-filtered air, which produced an $^{87}Sr/^{86}Sr$ ratio of 0.7087±0.0007 (n=1, 2-SE). Using this isotopic composition, blank subtraction of the measured Sr isotope compositions of the samples does not change the measured $^{87}Sr/^{86}Sr$ ratio more than 0.00001. We therefore consider blank contributions to be negligible. Importantly, because the $^{87}Sr/^{86}Sr$ ratio of the blank is lower than that of most samples analyzed in this study, blanks cannot be an explanation for the exceptionally radiogenic Sr isotope compositions measured in the Kuruman and Gamohaan formations.

Shale sampling and isotope analysis

Core samples of shale were first cleaned with ultra-pure water and acetone and placed in an ultrasonic bath for 15 minutes to remove contaminants. Shale layers were powdered and collected using a hand-held tungsten-carbide scribe, and ~80 mg of powder was collected for each sample. Powders were spiked with a mixed ^{87}Rb-^{84}Sr and mixed REE tracer (^{142}Ce-^{150}Nd-^{149}Sm-^{151}Eu-^{155}Gd-^{161}Dy-^{167}Er-^{171}Yb) prior to dissolution in distilled 29M HF and 14M HNO_3 (10:1 mix), followed by evaporation, and then redissolved in concentrated HCl. We note that we did not attempt to partially dissolve the shale samples to assess the isotopic compositions of labile Rb and Sr components (Ohr et al., 1991). The low grade of metamorphism, and accompanying phase transitions, makes it unlikely that currently leachable components would provide useful information on the labile Rb and Sr at the time of deposition. Rubidium, Sr, and the bulk REEs were separated using cation-exchange chromatography (BioRad AG 50W X 8

200-400 mesh resin) and 2.5M HCl as the mobile phase. The REE separations were made using 2-methylactic acid.

Isotopic analyses of shales followed that described above, with the following modifications. Strontium mass analysis used single Ta filaments with H_3PO_4, and a typical analysis consisted of 120 ratios and an ^{88}Sr ion intensity of $3x10^{-11}$ amps. Using the above method, 12 analyses of NIST SRM-987 Sr using 1.2 µg of Sr per analysis yielded an $^{87}Sr/^{86}Sr$ ratio of 0.71026±0.00002 (n=12, 2-SD). The measured $^{87}Sr/^{86}Sr$ ratios were corrected to initial $^{87}Sr/^{86}Sr$ ratios as described above. The Sr total procedural blank for shale analysis was 140 pg, which is negligible compared to sample Sr content.

Rubidium analyses of shales followed that described above, but used a different normalization ratio due to the higher quantities of Rb analyzed, relative to the carbonates. The measured $^{87}Rb/^{85}Rb$ of NIST SR-984 was 0.38248±0.00130 (n=3; 2-SD) on 3.5 µg loads of Rb. Relative to the certified Rb isotope composition of NIST SRM-984, this produces an exponential β correction factor of 0.3544, and this correction factor was applied to the measured $^{87}Rb/^{85}Rb$ ratios of the samples (Wasserburg et al., 1981). The Rb total procedural blank for shale analysis was 51 pg, which is negligible compared to sample Rb content.

Neodymium isotope analyses were performed as NdO^+ using a dynamic multi-collector analysis routine with Si-gel and H_3PO_4, and to further enhance NdO^+ formation the source can pressure was increased to 3×10^{-7} mbar by inletting O_2 via a gas bleed. Analyses ran 100 ratios at a $^{144}Nd^{16}O^+$ ion signal of 1×10^{-11} amps, and measured data were exponentially corrected for mass fractionation using $^{146}Nd/^{144}Nd = 0.7219$. Measurements of the UW AMES I and II and La Jolla standards yielded $^{143}Nd/^{144}Nd$ ratios of 0.512136±0.000021 (n=8, 2-SD), 0.511970±0.000017 (n=5, 2-SD), and 0.511844±0.000015 (n=6, 2-SD) respectively. Neodymium and samarium total procedural blanks were 119 pg and 245 pg respectively, which are negligible relative to samples.

Analysis of Sm and Nd contents were made by isotope dilution (ID) TIMS; Nd ID measurements were made during the full isotopic analysis noted above. Sm ID measurements were made on Ta filaments, using H_3PO_4, and Si-gel. Typical Sm analyses had ion signals of $1x10^{-12}$ amps and ran 50 ratios.

Elemental analysis

Each sampled lamina was examined by Heimann et al. (2010) for major-element chemistry by electron microprobe analysis (EMPA) on matching thin sections at the University of Wisconsin-Madison using a CAMECA SX51 electron microprobe with *Probe for Windows* software. Analyses were performed using an accelerating voltage of 15 kV and a Faraday cup current of 6 nA. Mineralogy of the carbonate laminae was determined by petrographic analysis, scanning electron microscope (SEM), back-scattered electron imaging (BSE), and energy dispersive spectrometry (EDS) using a Hitachi S03400 variable pressure SEM at the Department of Geoscience, University of Wisconsin-Madison. Using EMPA, carbonates were analyzed for Fe, Mg, Ca, and Mn contents, and CO_3 was calculated by difference, where 0.333 atoms of C were assigned per one oxygen atom, as calculated by charge balance. In addition, Si and Al were

analyzed to assess the presence of quartz or phyllosilicates coexisting with carbonates. Analyses that contained SiO_2 or Al_2O_3 contents >0.3 wt. %, effectively the detection limits of these elements by EMPA, identified carbonate that was not sampled for C, O, Fe, and Sr isotope analysis. Furthermore, carbonate bands that produced EMPA element totals <99% or >101% were not used, because such analyses could indicate the presence of non-carbonate minerals; using the CO_3 calculation noted above, no samples were taken if EMPA totals were outside 100±1%.

Error reporting

We assume a constant 0.5% error in the Rb/Sr ratio, which is based largely on the error in the measured $^{87}Rb/^{85}Rb$ ratio used for calculating the Rb concentration by ID. Because a mixed ^{84}Sr-^{87}Rb tracer was used, weighing errors will not affect the calculated Rb/Sr weight ratios. Errors in initial $^{87}Sr/^{86}Sr$ ratios are based on using the square root of the sum of the squares of the 2-SE in-run statistic and the change in the calculated initial $^{87}Sr/^{86}Sr$ ratio assuming, a 0.5% error in the Rb/Sr ratio. In addition, we incorporated an error of 10 m.y. in depositional age for calculation of the uncertainties in initial $^{87}Sr/^{86}Sr$ ratios. We used the ^{87}Rb decay constant determined by Nebel et al. (2011) of 1.393×10^{-11} y^{-1}.

Mineralogy and Petrology

Mineralogic and petrologic characterization of the sampled laminations was done to correlate possible relations between mineralogy and isotopic composition. The sampled BIF laminations contained siderite ($FeCO_3$) and ankerite ($[Ca,Fe,Mg]CO_3$) in varying proportions (Heimann et al., 2010), and bulk carbonate compositions of the material dissolved were calculated using mineral compositions determined by EMPA and the relative proportions of minerals determined by image analysis. Minor hematite inclusions are found in some siderite/ankerite grains, but these do not affect the Rb and Sr budgets. Siderite is typically ~5 μm in size, whereas ankerite is typically coarser grained at ~30 μm size. Ankerite grains often contain siderite inclusions, indicating siderite formed before ankerite. Both siderite and ankerite show no petrographic evidence of extensive post-lification recrystallization or alteration. A detailed description of sampled laminae, as well as major element compositions, is given in Heimann et al. (2010). In this paper we follow the conventions used by Heimann et al. (2010) in classifying these mixed carbonate compositions, where the term siderite is used if the majority of the carbonate is Fe rich and Ca and Mg poor, ankerite is used if the majority of the carbonate is a Ca- and Fe-rich carbonate, and calcite/dolomite is used if the majority of the carbonate is a Ca or Ca-Mg carbonate.

REFERENCES CITED

Beukes, N. J., and Gutzmer, J., 2008, Origin and paleoenvironmental signficance of major iron formations at the Archean-Paleoproterozoic boundary: Society of Economic Geologists SEG Reviews, v. 15, p. 5-47.

Beukes, N. J., and Klein, C., 1990, Geochemistry and Sedimentology of a Facies Transition - from Microbanded to Granular Iron-Formation - in the Early Proterozoic Transvaal Supergroup, South-Africa: Precambrian Research, v. 47, no. 1-2, p. 99-139.

Beukes, N. J., Klein, C., Kaufman, A. J., and Hayes, J. M., 1990, Carbonate Petrography, Kerogen Distribution, and Carbon and Oxygen Isotope Variations in an Early Proterozoic Transition from Limestone to Iron-Formation Deposition, Transvaal Supergroup, South-Africa: Economic Geology and the Bulletin of the Society of Economic Geologists, v. 85, no. 4, p. 663-690.

Carothers, W. W., Adami, L. H., and Rosenbauer, R. J., 1988, Experimental oxygen isotope fractionation between siderite-water and phosphoric acid liberated CO_2-siderite: Geochimica et Cosmochimica Acta, v. 52, p. 2445-2450.

Charlier, B. L. A., Ginibre, C., Morgan, D., Nowell, G. M., Pearson, D. G., Davidson, J. P., and Ottley, C. J., 2006, Methods for the microsampling and high-precision analysis of strontium and rubidium isotopes at single crystal scale for petrological and geochronological applications: Chemical Geology, v. 232, p. 114-133.

Fischer, W. W., Schroeder, S., Lacassie, J. P., Beukes, N. J., Goldberg, T., Strauss, H., Horstmann, U. E., Schrag, D. P., and Knoll, A. H., 2009, Isotopic constraints on the Late Archean carbon cycle from the Transvaal Supergroup along the western margin of the Kaapvaal Craton, South Africa: Precambrian Research, v. 169, p. 15-27.

Heimann, A., Johnson, C. M., Beard, B. L., Valley, J. W., Roden, E. E., Spicuzza, M. J., and Beukes, N. J., 2010, Fe, C, and O isotope compositions of banded iron formation carbonates demonstrate a major role for dissimilatory iron reduction in similar to 2.5 Ga marine environments: Earth and Planetary Science Letters, v. 294, no. 1-2, p. 8-18.

Jimenez-Lopez, C., Caballero, E., Huertas, F. J., and Romanek, C. S., 2001, Chemical, mineralogical and isotope behavior, and phase transformation during the precipitation of calcium carbonate minerals from intermediate ionic solution at 25 ^{o}C: Geochimica et Cosmochimica Acta, v. 65, p. 3219-3231.

Jimenez-Lopez, C., and Romanek, C. S., 2004, Precipitation kinetics and carbon isotope partitioning of inorganic siderite at 25 ^{o}C and 1 atm: Geochimica et Cosmochimica Acta, v. 68, p. 557-571.

Johnson, C. M., Beard, B. L., Beukes, N. J., Klein, C., and O'Leary, J. M., 2003, Ancient geochemical cycling in the Earth as inferred from Fe isotope studies of banded iron formations from the Transvaal Craton: Contributions to Mineralogy and Petrology, v. 144, no. 5, p. 523-547.

Kamber, B. S., and Webb, G. E., 2001, The geochemistry of late Archaean microbial carbonate: Implications for ocean chemistry and continental erosion history: Geochimica Et Cosmochimica Acta, v. 65, no. 15, p. 2509-2525.

Kaufman, A. J., 1996, Geochemical and mineralogic effects of contact metamorphism on banded iron-formation: an example from the Transvaal Basin, South Africa: Precambrian Research, v. 79, p. 171-194.

Kim, S.-T., and O'Neil, J. R., 1997, Equilibrium and nonequilibrium oxygen isotope effects in synthetic carbonates: Geochimica et Cosmochimica Acta, v. 61, p. 3461-3475.

Klein, C., and Beukes, N. J., 1989, Geochemistry and Sedimentology of a Facies Transition from Limestone to Iron-Formation Deposition in the Early Proterozoic Transvaal Supergroup, South-Africa: Economic Geology, v. 84, no. 7, p. 1733-1774.

Nebel, O., Scherer, E. E., and Mezger, K., 2011, Evaluation of the ^{87}Rb decay constant by age comparison against the U-Pb system: Earth and Planetary Science Letters, v. 301, p. 1-8.

Ohr, M., Halliday, A. N., and Peacor, D. R., 1991, Sr and Nd isotopic evidence for punctuated clay diagenesis, Texas Gulf coast: Earth and Planetary Science Letters, v. 105, p. 110-126.

Shields, G. A., and Veizer, J., 2002, The Precambrian marine carbonate isotope database: version 1.1: Geochemistry, Geophysics, Geosystems, v. 3, no. 6.

Valaas-Hyslop, E., Valley, J. W., Johnson, C. M., and Beard, B. L., 2008, The effects of metamorphism on O and Fe isotope compositions in the Biwabik iron-formation, northern Minnesota: Contributions to Mineralogy and Petrology, v. 155, p. 313-328.

Veizer, J., 1989, Strontium isotopes in seawater through time: Annual Review in Earth and Planetary Sciences, v. 17, p. 141-167.

Von Blanckenburg, F., Mamberti, M., Schoenberg, R., Kamber, B. S., and Webb, G. E., 2008, The iron isotope composition of microbial carbonate: Chemical Geology, v. 249, p. 113-128.

Wasserburg, G. J., Jacobsen, S. B., DePaolo, D. J., McCulloch, M. T., and Wen, T., 1981, Precise determination of Sm/Nd ratios, Sm and Nd isotopic abundances in standard solutions: Geochimica Et Cosmochimica Acta, v. 45, p. 2311-2323.

Wiesli, R. A., Beard, B. L., and Johnson, C. M., 2004, Experimental determination of Fe isotope fractionation between aqueous Fe(II), siderite and "green rust" in abiotic systems: Chemical Geology, v. 211, no. 3-4, p. 343-362.

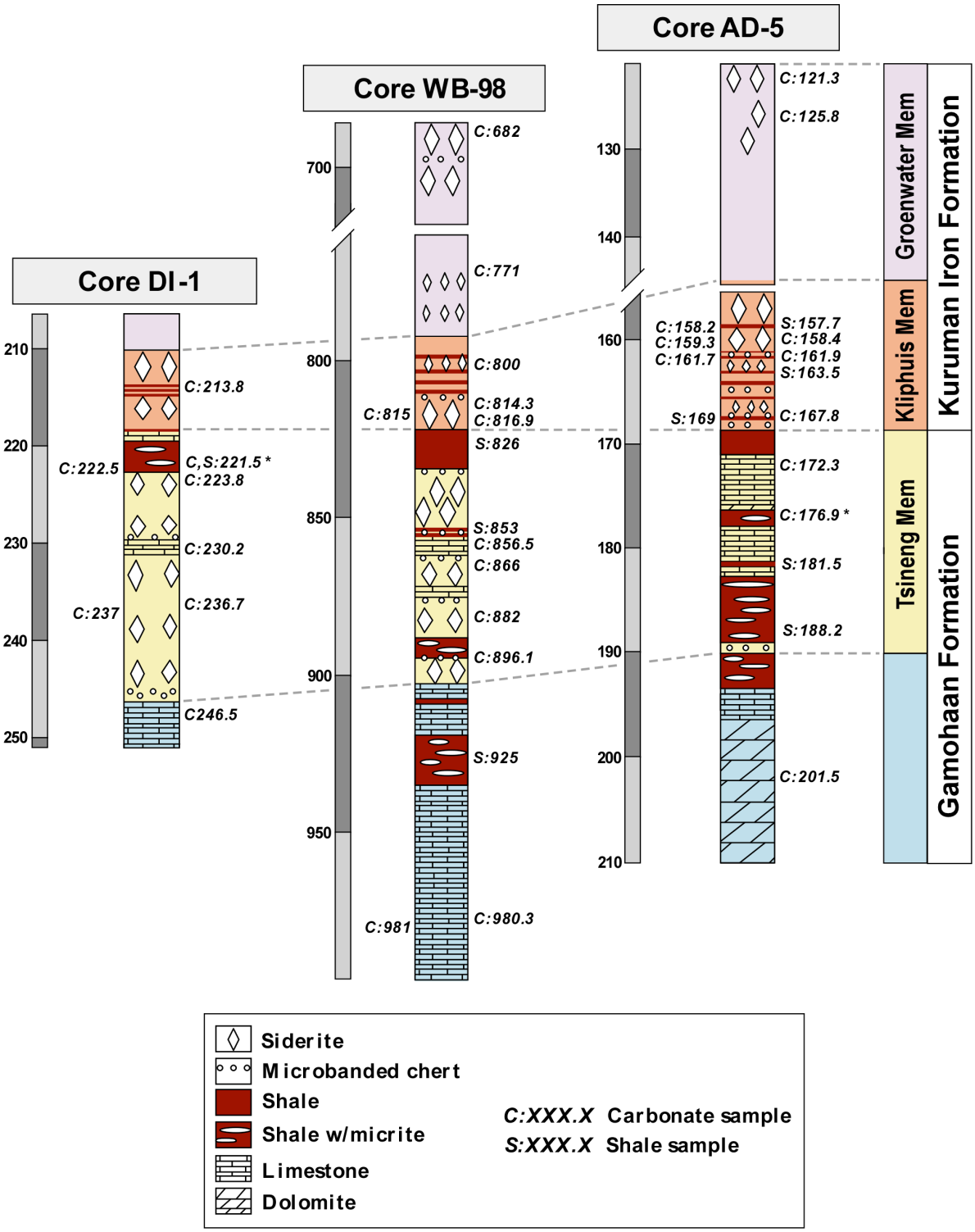

Figure DR-1. Simplified lithostratigraphic profiles for cores DI-1, WB-98, and AD-5, which reflects a SW-NE transect across the Campbellrand platform, Transvaal Basin, South Africa. The sequence of rocks encompasses the ~2.5 Ga transition from the shallow water Ca-Mg carbonates of the Gamohaan Formation to the deep water, Fe-rich Kuruman Iron Formation. Lithostratigraphy modified from Klein and Beukes (1989). Figure modified from Heimann et al. (2010). Profiles are in meters for DI-1 and AD-5 and in feet for WB-98. Samples analyzed in this study (Tables DR-1 and DR-2) are noted at appropriate depths, where "C" prefix indicates carbonate sample, and "S" prefix indicates shale sample. "*" notes carbonate sampled within a shale layer.

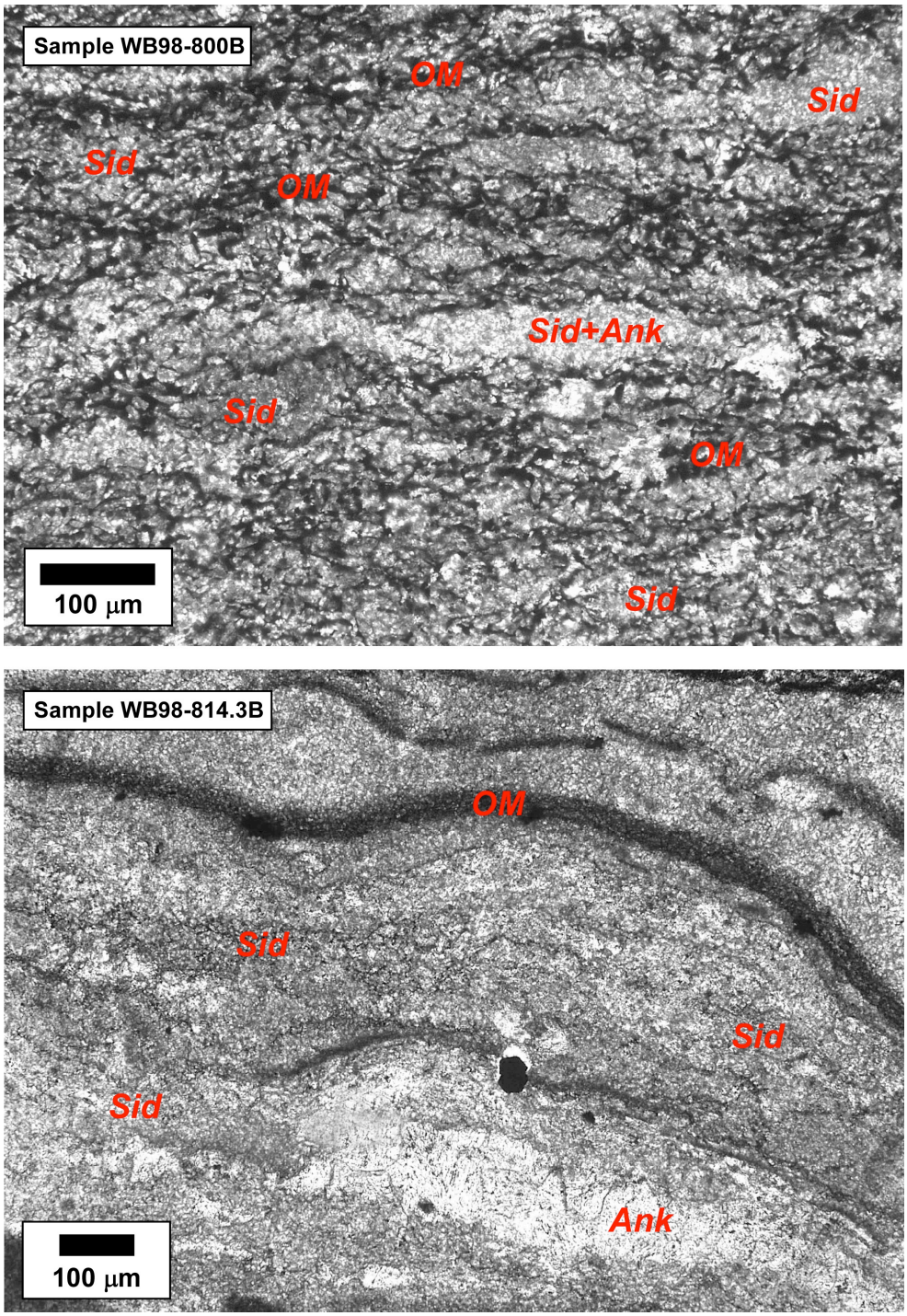

Figure DR-2. Representative photomicrographs of carbonates in the Kuruman Iron Formation. Upper image shows sample that is dominated by siderite (Sid). Lower image illustrates sample that contains early siderite and later ankerite (Ank). Siderite is fine-grained and is interpreted to be an early phase in all samples based on distribution parallel to bedding, including organic matter (OM) and chert layers, and the lack of coarse-grained textures or cross-cutting veins that would indicate later recrystallization. Ankerite may also occur as an early phase, but may also occur as isolated, coarser-grained components, and ankerite may replace siderite laminations; these features are indicative of very early diagenetic changes prior to lithification. Importantly, the isotopic compositions of ankerite and siderite in this study overlap, indicating that they broadly record similar isotopic components. In no case is there petrographic evidence for pervasive, regional mineralization or recrystallization significantly after lithification.

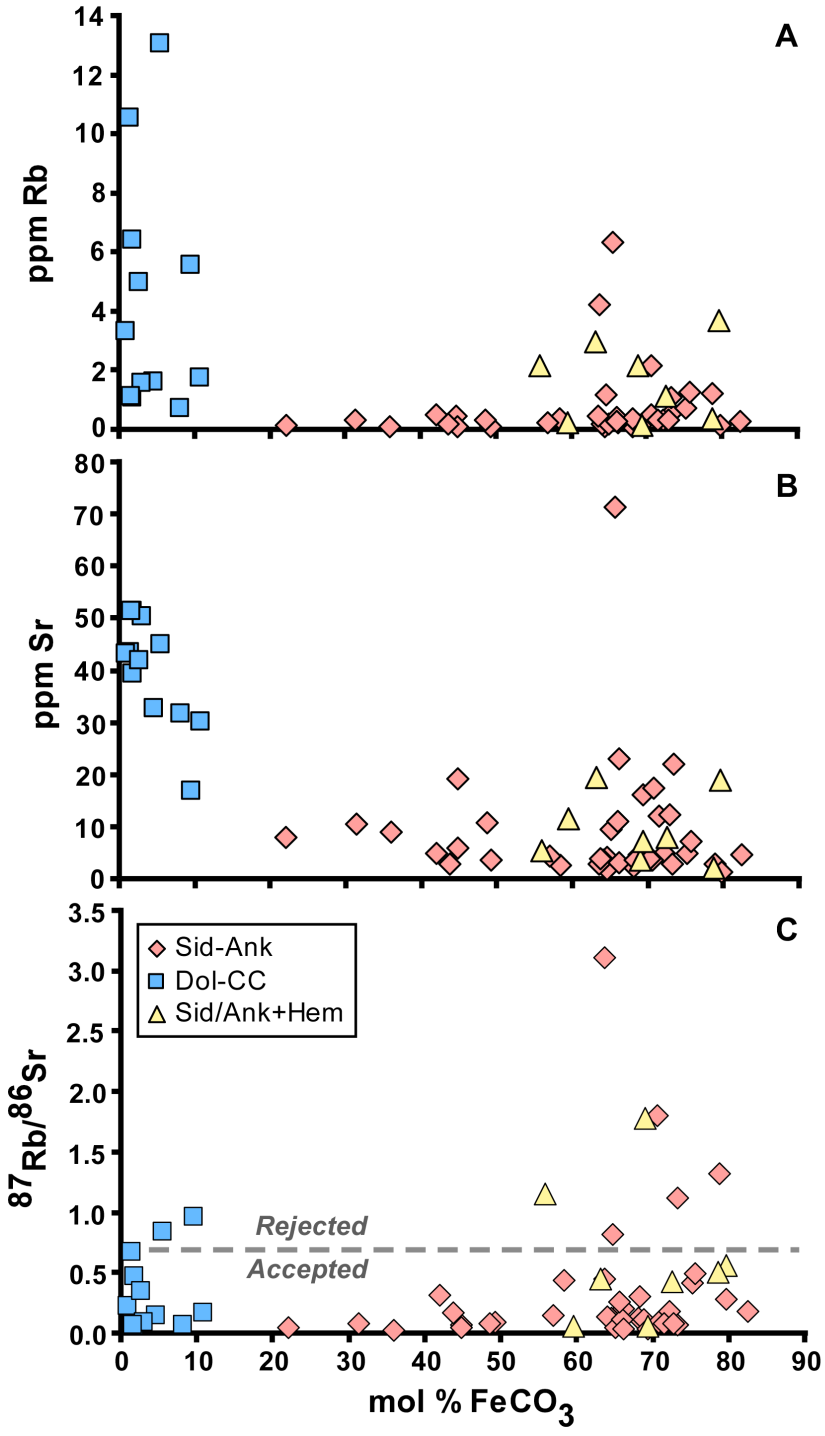

Figure DR-3. Rb and Sr contents determined by isotope dilution for all carbonate samples in Table DR-1, relative to mol % $FeCO_3$ contents determined by electron microprobe analysis. These analyses reflect sampling only those carbonate bands that contained less than 0.5 wt. % Al_2O_3 contents (determined by electron microprobe analysis), as a first pass to filter for siliciclastic contamination. Based on $^{87}Rb/^{86}Sr$ variations (part C), we apply a further filter, excluding discussion of results where $^{87}Rb/^{86}Sr>0.75$.

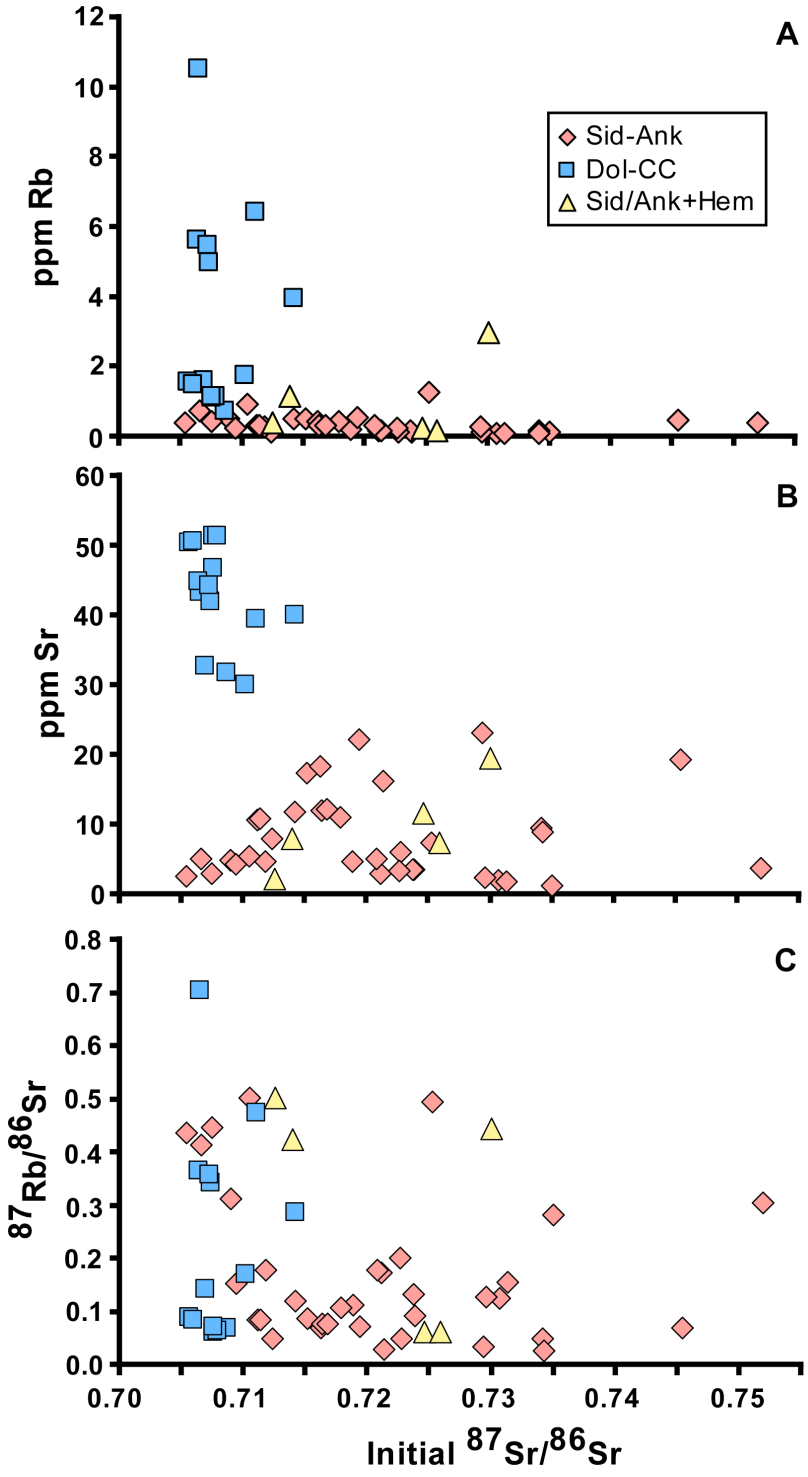

Figure DR-4. Rb and Sr contents versus initial $^{87}Sr/^{86}Sr$ ratios for samples that contain $^{87}Rb/^{86}Sr<0.75$. The lack of correlations between Rb contents and $^{87}Rb/^{86}Sr$ ratios and initial $^{87}Sr/^{86}Sr$ ratios provides strong evidence that Sr isotope compositions of this sample suite is not affected by siliciclastic contamination, and instead reflects the Sr isotope composition of the carbonates when they formed. Note that a single Ca-Mg sample (AD-5-176.9) has a very radiogenic initial $^{87}Sr/^{86}Sr$ ratio of 0.7771, but this sample is finely interlayered with shale at the mm to cm scale, and so would have been susceptible to any post-depositional Sr mobility over short distances, and this sample will not be considered further, nor is it plotted in any diagram.

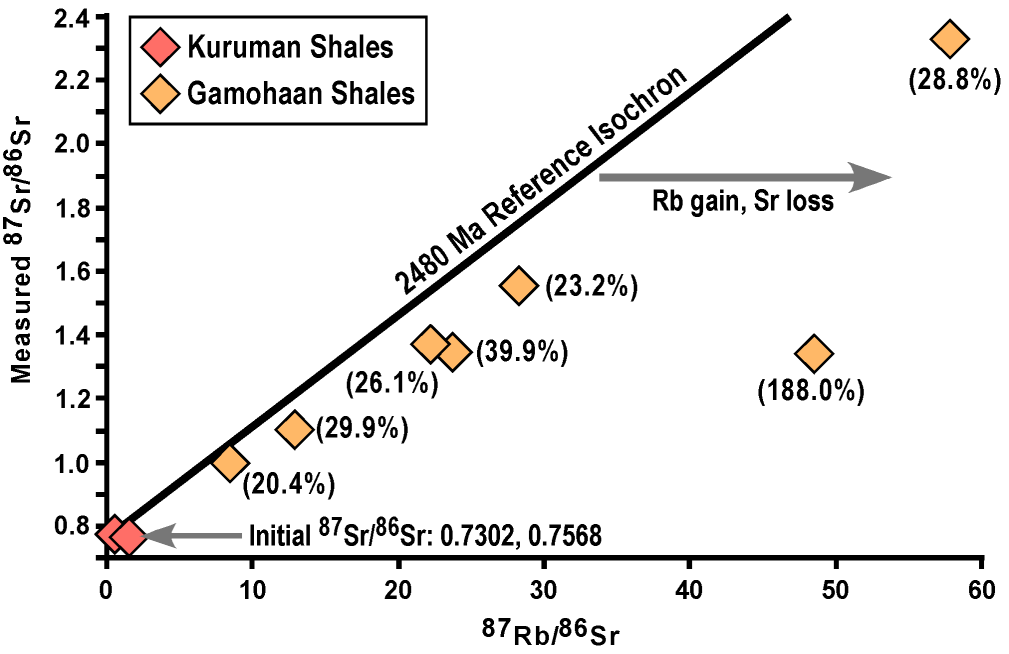

Figure DR-5. Measured $^{87}Sr/^{86}Sr$-$^{87}Rb/^{86}Sr$ isochron diagram for shale samples from the Gamohaan and Kuruman formations. The Kuruman IF samples come from thin shale beds in the IF, which is the typical occurrence of shale in this unit. These have calculated initial $^{87}Sr/^{86}Sr$ ratios (at 2480 Ma) that lie within the range analyzed for Fe-rich carbonates from the Kuruman IF. In contrast, the shale samples form the Gamohaan Formation have much higher $^{87}Rb/^{86}Sr$ ratios. Shale in this unit generally occurs as thick sections of siliciclastic rocks. All of the Gamohaan shale samples have very high measured $^{87}Sr/^{86}Sr$ ratios, but all fall off a 2480 Ma reference isochron, suggesting some Rb mobility (% Rb gain noted in parentheses).

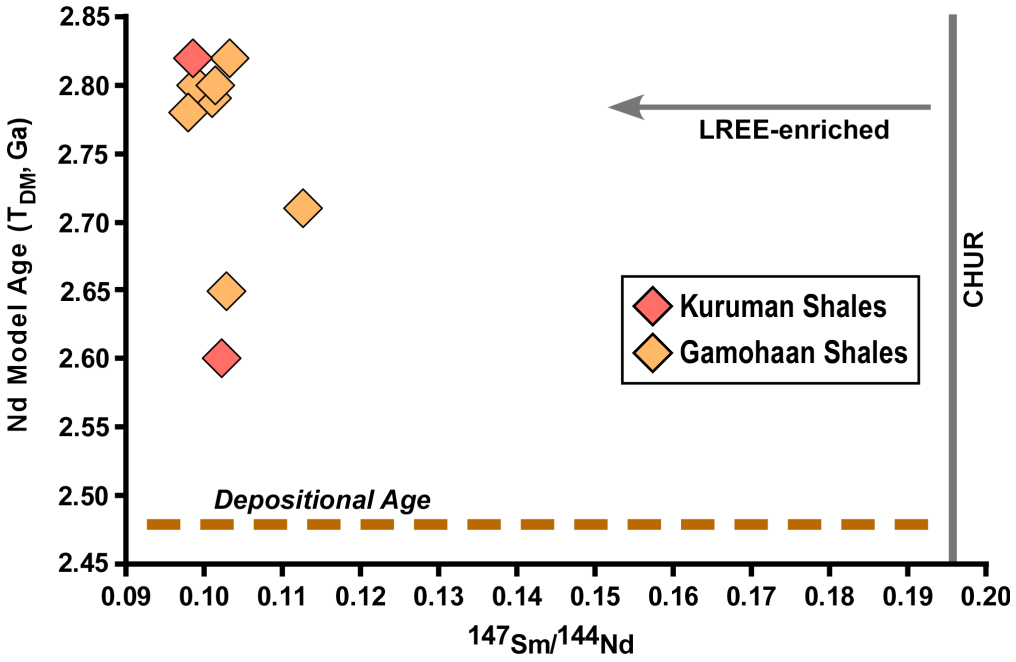

Figure DR-6. ^{147}Sm-^{143}Nd isotope data for shale samples shown in Figure DR-5. All samples have LREE-enrichment (low $^{147}Sm/^{144}Nd$) that is typical of continentally-derived shales, significantly lower than the Chondrite Uniform Reservoir (CHUR). Moreover, Nd model ages, calculated assuming a depleted mantle (T_{DM}), are all older than the 2480 Ma depositional age, indicating derivation from older sources. As such, the shales likely had high $^{87}Sr/^{86}Sr$ ratios at the time of deposition, although this is difficult to directly infer from the measured $^{87}Rb/^{86}Sr$-$^{87}Sr/^{86}Sr$ relations (Figure DR-5) due to Rb mobility in the Gamohaan samples.

Table DR-1: Chemical and C, O, Fe, and Rb-Sr isotope compositions of carbonates

Sample	Lamination	Mineralogy	$\delta^{18}O$	$\delta^{13}C$	$\delta^{56}Fe$	Avg. mol %			Rb	Sr	$^{87}Rb/^{86}Sr$	$^{87}Sr/^{86}Sr$	± (2SE)	$^{87}Sr/^{86}Sr$	± (2SE)
			‰ (SMOW)	‰ (PDB)	‰ (lgRxs)	$FeCO_3$	$MgCO_3$	$CaCO_3$	ppm	ppm		measured		initial	
AD-5-121.3	*lamination 1a*	sid-ank-py	20.07	-6.4	-0.85	64.66	17.56	17.78	1.16	4.13	0.81489	0.73604	0.00003		
AD-5-121.3	*lamination 3*	sid-ank-py	20.38	-6.99	-0.84	78.80	16.60	4.60	1.23	2.70	1.32183	0.73713	0.00021		
AD-5-121.3	*lamination 7*	sid-ank-py	20.05	-7.25	-0.72	79.74	16.02	4.25	0.12	1.24	0.28101	0.74490	0.00008	0.73502	0.00013
AD-5-158.2A	*lamination 4*	ank-sid			-0.64	44.79	22.38	32.83	0.45	19.25	0.06790	0.74789	0.00003	0.74550	0.00004
AD-5-158.2A	*lamination 7*	ank	19.55	-3.13	-1.05	22.11	24.25	53.64	0.13	7.92	0.04752	0.71409	0.00001	0.71242	0.00002
AD-5-158.2A	*lamination 9*	ank=sid	19.71	-4.14	-0.64	49.28	22.53	28.19	0.11	3.51	0.09084	0.72704	0.00003	0.72385	0.00004
AD-5-158.4B	*lamination 4*	sid-ank	20.42	-5.31	-0.2	64.54	18.81	16.65	0.08	1.86	0.12478	0.73514	0.00003	0.73075	0.00005
AD-5-158.4B	*lamination 4*								0.09	1.70	0.15361	0.73676	0.00002	0.73136	0.00005
AD-5-159.3	*lamination 1*	sid-ank	20.11	-4.52	-0.51	64.11	23.83	12.06	0.16	3.52	0.13178	0.72840	0.00004	0.72377	0.00006
AD-5-159.3	*lamination 12*	sid-ank	20.47	-4.39	-0.47	65.03	22.37	12.60	0.16	9.48	0.04897	0.73590	0.00003	0.73418	0.00004
AD-5-161.7A	*lamination 2*	sid-ank	20.23	-4.56	-0.43	68.10	21.56	10.34	0.10	2.31	0.12557	0.73398	0.00011	0.72957	0.00013
AD-5-161.7A	*lamination 5*	sid-ank	19.53	-4	-0.51	44.86	21.80	33.34	0.10	5.92	0.04895	0.72450	0.00003	0.72278	0.00004
AD-5-161.7A	*lamination 6*	ank-sid	19.34	-3.42	-0.61	35.96	24.70	39.34	0.08	8.86	0.02619	0.73515	0.00002	0.73423	0.00002
AD-5-161.9A	*lamination 2*	sid	21.16	-4.99	-0.12	82.45	16.83	0.72	0.28	4.59	0.17667	0.71804	0.00001	0.71183	0.00004
AD-5-161.9A	*lamination 3*	sid-ank	20.47	-5.07	-0.13	68.81	19.60	11.59	0.18	4.69	0.11121	0.72283	0.00032	0.71892	0.00034
AD-5-161.9A	*lamination 4*	ank-sid	19.63	-2.73	-0.52	31.37	24.25	44.38	0.30	10.52	0.08256	0.71411	0.00005	0.71121	0.00006
AD-5-167.8B	*lamination 2*	sid=ank	18.69	-4.82	0.58	43.71	22.07	34.21	0.17	2.85	0.17291	0.72726	0.00004	0.72118	0.00007
AD-5-167.8B	*lamination 4*	sid-ank	19.41	-4.79	-0.17	66.14	21.18	12.68	0.22	3.18	0.20059	0.72969	0.00002	0.72264	0.00005
AD-5-167.8B	*lamination 5b*	sid=ank	19.19	-4.3	0.01	48.64	22.94	28.42	0.31	10.79	0.08318	0.71435	0.00004	0.71143	0.00005
AD-5-172.3	*lamination 1*	cal-dol	19.78	-1.27	-0.85	1.79	3.67	94.54	6.43	39.38	0.47334	0.72773	0.00001	0.71109	0.00009
AD-5-172.3	*lamination 1*								3.96	40.09	0.28625	0.72425	0.00001	0.71419	0.00006
AD-5-172.3	*lamination 5*	cal-dol	19.56	-1.35	-1.02	1.48	3.63	94.90	10.53	43.34	0.70457	0.73126	0.00039	0.70649	0.00050
AD-5-176-9	*lamination 1*	cal-py	19.63	-2.59	-1	0.89	0.50	98.61	3.32	43.09	0.22461	0.78502	0.00002	0.77713	0.00006
AD-5-201.5	*sample 1*	dol			-1.3	4.60	39.97	55.43	1.60	32.62	0.14197	0.71188	0.00002	0.70689	0.00004
DI-1-213.8B	*lamination 4*	sid-ank-py	19.48	-6.15	-0.77	73.35	13.82	12.83	0.54	22.08	0.07086	0.72194	0.00001	0.71945	0.00002
DI-1-213.8B	*lamination 5*	sid-ank-py	19.41	-6.72	-0.75	69.37	13.97	16.66	0.16	16.08	0.02883	0.72234	0.00039	0.72133	0.00039
DI-1-213.8C	*lamination 3*	sid-ank-py	19.96	-5.91	-0.87	72.22	15.13	12.65	0.30	4.94	0.17604	0.72699	0.00015	0.72080	0.00018
DI-1-213.8C	*lamination 7*	sid-ank-py	20.17	-5.71	-0.89	66.03	16.51	17.46	0.40	10.87	0.10661	0.72170	0.00003	0.71795	0.00005
DI-1-213.8C	*lamination 7*								0.48	11.70	0.11882	0.71836	0.00001	0.71418	0.00003
DI-1-221.5	*lamination 1*	sid-ank	21.32	-3.97	-0.05	73.28	16.81	9.90	1.07	2.78	1.12093	0.77507	0.00002		
DI-1-222.5	*lamination 5*	sid-ank	21.58	-4.55	-0.08	68.22	17.83	13.95	0.38	3.64	0.30367	0.76268	0.00007	0.75201	0.00012
DI-1-223.8A	*lamination 1*	ank-sid			0.07	42.05	20.99	36.96	0.51	4.76	0.31036	0.71988	0.00004	0.70897	0.00009
DI-1-223.8B	*lamination 1*	sid-ank	20.33	-4.98	0.09	63.59	19.22	17.20	0.43	2.79	0.44659	0.72320	0.00003	0.70750	0.00010
DI-1-230.2	*lamination 1*	dol-cal	20.74	-0.85	-0.1	10.80	16.61	72.60	1.75	30.09	0.16841	0.71612	0.00001	0.71020	0.00004
DI-1-230.2	*lamination 2*	dol-cal	19.85	-1.15	-0.09	8.18	11.54	80.27	0.74	31.79	0.06737	0.71104	0.00001	0.70867	0.00002
DI-1-236.7A	*lamination 2*	sid-hem	20.64	-7.63	0.32	79.62	17.85	2.54	3.69	18.99	0.56262	0.71548	0.00004		
DI-1-236.7A	*lamination 3*	sid-ank-hem	20.66	-7.31	0.23	68.94	18.70	12.36	2.14	3.49	1.78062	0.74533	0.00004		
DI-1-236.7B	*lamination 1*	sid-ank			-0.11	70.56	17.55	11.89	2.17	3.50	1.79812	0.73219	0.00015		
DI-1-237	*lamination 3*	sid-ank	21.25	-6.91	0.25	63.71	19.20	17.08	4.23	3.94	3.11226	0.72762	0.00006		
DI-1-237	*lamination 4*	sid-ank	21.68	-6.7	0.16	58.40	18.96	22.64	0.37	2.46	0.43572	0.72073	0.00041	0.70541	0.00048
DI-1-237	*lamination 8*	sid-ank-OM	20.73	-6.64	0.21	56.93	20.33	22.74	0.22	4.22	0.15094	0.71475	0.00028	0.70944	0.00030
DI-1-246.5	*lamination 1*	cal	20.82	-0.74	-0.59	1.77	1.00	97.23	1.09	51.30	0.06149	0.70971	0.00001	0.70755	0.00002
DI-1-246.5	*lamination 2*	cal-dol	21.14	-0.63	-0.75	2.98	2.71	94.31	1.55	50.40	0.08899	0.70877	0.00002	0.70564	0.00003
DI-1-246.5	*lamination 2*								1.47	50.58	0.08410	0.70895	0.00031	0.70599	0.00032
DI-1-246.5	*lamination 4*	cal	20.87	-0.71	-0.58	1.60	0.86	97.54	1.13	51.41	0.06361	0.71014	0.00004	0.70790	0.00005
DI-1-246.5	*lamination 4*								1.14	46.68	0.07067	0.71008	0.00002	0.70760	0.00003
WB98-771A-c	*sample 1*	sid-ank	20.38	-8.8		65.57	12.10	22.33	6.32	71.29	0.25682	0.72055	0.00002		
WB98-800A	*lamination 5*	sid-ank	20.26	-7.16	-0.15	70.71	12.79	16.49	0.51	17.37	0.08504	0.71823	0.00002	0.71524	0.00003
WB98-800A	*lamination 5*								0.43	18.22	0.06836	0.71863	0.00002	0.71623	0.00003
WB98-800B	*lamination 2*	sid-ank-OM	20.78	-6.76	-0.57	71.54	15.66	12.80	0.31	12.00	0.07482	0.71896	0.0003	0.71633	0.00031
WB98-800B	*lamination 5*	sid-ank-OM	20.45	-6.47	-0.39	72.83	14.32	12.86	0.32	12.15	0.07629	0.71951	0.00001	0.71683	0.00002
WB98-800C-G	*lamination 1*	sid-ank	21.42	-6.48	-0.29	75.24	14.14	10.62	0.71	4.98	0.41303	0.72114	0.00014	0.70662	0.00021
WB98-800C-G	*lamination 3*	sid-ank	21.47	-6.92	-0.17				0.93	5.39	0.50020	0.72807	0.00005	0.71049	0.00013
WB98-814.3A	*lamination 2*	sid-ank	19.71	-7.1	0.47	66.13	16.84	17.03	0.26	23.04	0.03272	0.73057	0.00002	0.72942	0.00003
WB98-815A	*lamination 1*	sid-ank	20.03	-6.66	0.23	75.66	16.84	7.49	1.24	7.28	0.49449	0.74267	0.00001	0.72529	0.00009
WB98-816.9	*lamination 4*	sid-ank	19.46	-6.74	0.57	70.25	17.24	12.51		3.89		0.76366	0.00002		
WB98-856.5	*lam./area 2*	dol-cal	20.72	-1.64	0.13	9.54	18.94	71.53	5.56	16.85	0.95858	0.74933	0.00002		
WB98-866A	*lamination 5*	sid-ank-hem	20.45	-4.48	0.94	59.55	15.19	25.26	0.24	11.46	0.06070	0.72678	0.00003	0.72465	0.00004
WB98-866A	*lamination 9*	sid-ank-hem	19.91	-4.65	0.83	69.33	16.67	14.00	0.15	7.22	0.06023	0.72801	0.00004	0.72589	0.00005
WB98-866A	*lamination 10*	sid-ank-hem	20.18	-4.32	0.69	63.18	17.47	19.35	2.96	19.37	0.44377	0.74564	0.00012	0.73004	0.00019
WB98-866A	*lamination 14*	sid-ank-hem	20.35	-4.67	0.73	78.70	17.23	4.07	0.37	2.14	0.50133	0.73016	0.00011	0.71254	0.00019
WB98-882	*lamination 1*	sid-ank-hem	21.66	-5.68	0.62	72.49	14.88	12.63	1.14	7.80	0.42374	0.72886	0.00008	0.71397	0.00015
WB98-896.1B	*lamination 7*	sid-ank-hem	20.64	-4.98	0.76	55.86	20.48	23.66	2.17	5.48	1.15466	0.78775	0.00035		
WB98-980.3	*sample 1*	cal-dol-py	21.36	-1.16	-1.66	5.50	5.31	89.19	13.07	44.98	0.84270	0.73197	0.00002		
WB98-980.3	*sample 1*								5.63	44.84	0.36368	0.71919	0.00001	0.70641	0.00007
WB98-981	*lamination 1*	cal-py	21.25	-1.19	-1.45	2.65	0.59	96.75	4.96	41.97	0.34231	0.71938	0.00001	0.70735	0.00006
WB98-981	*lamination 1*								5.45	44.18	0.35733	0.71978	0.00002	0.70722	0.00008

Notes: O, C, and Fe isotope data, and chemical compositions, from Heimann et al. (2010). Rb-Sr isotope data and concentrations from this study.

Table DR- 2: Rb-Sr and Sm-Nd isotope data for shales

Sample	Rb ppm	Sr ppm	% Rb gain	87Rb/86Sr	87Sr/86Sr measured	± (2SE)	87Sr/86Sr initial	± (2SE)	Sm ppm	Nd ppm	147Sm/144Nd	143Nd/144Nd measured	Eps Nd(t)	T-DM (Ga)
AD-5-188.2	57.82	13.43	29.93	12.93519	1.1007	0.00003			3.55	19.27	0.102944	0.511213	1.85	2.65
AD-5-181.5	68.02	3.94	28.83	57.87507	2.32978	0.00003			3.16	17.49	0.101015	0.511076	-0.24	2.79
AD-5-163.5	2.62	14.74	0.00	0.51765	0.77497	0.00003	0.75677	0.00012	2.17	12.31	0.098647	0.511008	-0.82	2.82
AD-5-157.7	0.68	2.06	0.00	0.96031	0.76392	0.00003	0.73017	0.00019	6.92	37.84	0.102168	0.51124	2.63	2.6
AD-5-169	105.08	13.59	39.92	23.77132	1.34751	0.00003			3.13	17.67	0.098978	0.511034	-0.41	2.8
WB-98-826	21.17	1.34	188.03	48.53581	1.33985	0.00003			6.21	35.43	0.097928	0.511027	-0.21	2.78
WB-98-853	143.09	19.82	26.07	22.24091	1.3699	0.00003			2.93	16.13	0.101492	0.511077	-0.36	2.8
WB-98-925	199.03	22.08	23.24	28.24197	1.55513	0.00003			3.42	18.49	0.103311	0.511094	-0.61	2.82
DI-1-221.5	66.44	23.31	20.36	8.48130	0.99865	0.00003			2.75	13.66	0.112719	0.511348	1.38	2.71

Notes: ε_{Nd} (T) are relative to CHUR calculated at 2480 Ma. TCHUR was calculated using a CHUR $^{143}Nd/^{144}Nd = 0.512638$ and $^{147}Sm/^{144}Nd = 0.1966$, T_{DM} was calculated using depleted mantle $^{143}Nd/^{144}Nd = 0.51315$ and $^{147}Sm/^{144}Nd = 0.2136$.